AGU PUBLICATIONS

Geophysical Research Letters

RESEARCH LETTER
10.1002/2016GL069005

Key Points:
- Entrainment rate of a plume is dependent on its vertical velocity and distance to cloud edge
- Changes in stratification and buoyancy, buoyancy gradient, etc. have little effect on entrainment rate
- Entrainment per unit time in cumulus clouds does not depend on vertical velocity

Supporting Information:
- Supporting Information S1

Correspondence to:
Y. Tian,
yangtian@fas.harvard.edu

Citation:
Tian, Y., and Z. Kuang (2016), Dependence of entrainment in shallow cumulus convection on vertical velocity and distance to cloud edge, *Geophys. Res. Lett.*, *43*, 4056–4065, doi:10.1002/2016GL069005.

Received 30 JAN 2016
Accepted 11 APR 2016
Accepted article online 18 APR 2016
Published online 30 APR 2016

Dependence of entrainment in shallow cumulus convection on vertical velocity and distance to cloud edge

Yang Tian[1] and Zhiming Kuang[1,2]

[1]Department of Earth and Planetary Sciences, Harvard University, Cambridge, Massachusetts, USA, [2]John A. Paulson School of Engineering and Applied Sciences, Harvard University, Cambridge, Massachusetts, USA

Abstract The dependence of entrainment rate on environmental conditions and cloud characteristics is investigated using large eddy simulations (LES) of the response of shallow cumulus convection to a small-amplitude temperature perturbation that is horizontally uniform and localized in height. The simulated cumulus fields are analyzed in the framework of an ensemble of entraining plumes by tracking a large number of Lagrangian parcels embedded in the LES and grouping them into different plumes based on their detrainment heights. The results show that fractional entrainment rate per unit height of a plume is inversely proportional to the plume's vertical velocity and its distance to the cloud edge, while changes in environmental stratification and relative humidity, the plume's buoyancy, or the vertical gradient of its buoyancy due to the temperature perturbation have little effect on the plume's entrainment rate.

1. Introduction

How entrainment processes in cumulus clouds depend on environmental conditions and cloud characteristics has been an active area of research, and choices of such dependence in cumulus parameterization schemes are highly consequential to each scheme's behavior and the simulated large-scale weather and climate [e.g., *Grant and Brown*, 1999; *Gregory*, 2001; *Neggers et al.*, 2002; *Bechtold et al.*, 2008; *Chikira and Sugiyama*, 2010; *Mapes and Neale*, 2011; *Dawe and Austin*, 2013].

In discussing entrainment, it is important to specify the conceptual model within which entrainment is defined. The most widely used models include the bulk entraining-detraining plume model, where the cumulus ensemble is represented by a single bulk plume [e.g., *Tiedtke*, 1989], and the spectral entraining plume ensemble model, where the cumulus ensemble is represented by a spectrum of entraining plumes with different entrainment characteristics [e.g., *Arakawa and Schubert*, 1974], as well as different formulations of multiparcel models [e.g., *Raymond and Blyth*, 1986; *Nie and Kuang*, 2012a; *Neggers et al.*, 2002]. Drawing from theories of similarity plumes such as *Morton et al.* [1956], an inverse relationship between the fractional entrainment rate per unit height (Unless specified otherwise, fractional entrainment rate throughout this paper refers to fractional entrainment rate per unit height.) $\epsilon = \mathrm{d}\,ln(M)/\mathrm{d}z$ (where M is the mass flux and z is height) and cloud size R, i.e., $\epsilon \propto \frac{1}{R}$, has been often used in bulk entraining-detraining plume models [e.g., *Simpson and Wiggert*, 1969; *Tiedtke*, 1989; *Siebesma*, 1998; *Bretherton et al.*, 2004]. As cloud size tends to be larger for deeper clouds, some authors have proposed, again in the context of a bulk entraining-detraining plume model, to tie ϵ to the height of the cloud, as $\epsilon \propto 1/z$ [e.g., *Siebesma*, 1998] or with other empirically fitted formulae [*Hohenegger and Bretherton*, 2011]. *Neggers et al.* [2002] suggested that in their multiple-parcel model, the fractional entrainment rate of a parcel is inversely proportional to the parcel's vertical velocity. This formulation is further applied to a spectral entraining plume ensemble model by *Chikira and Sugiyama* [2010]. There are also ideas that relate ϵ to thermodynamical properties: based on earlier modeling work by *Bretherton and Smolarkiewicz* [1989], *Emanuel and Zivkovic-Rothman* [1999] argued in general terms that entrainment should increase with increasing vertical gradient of plume buoyancy ($\mathrm{d}b/\mathrm{d}z$, where b is the plume buoyancy) because of the inflow associated with such a gradient, whereas *Lin* [1999] suggested that within an ensemble of entraining plumes, plumes with smaller buoyancy have larger entrainment rates, and *Bechtold et al.* [2008] suggested that in the context of a bulk entraining-detraining plume model, ϵ increases with decreasing environmental relative humidity. *Gregory* [2001] suggested a formulation where the entrainment rate of a bulk plume is proportional to its buoyancy and inversely proportional to the square of its vertical velocity. This formulation was further used in an entraining plume ensemble model by *Chikira and Sugiyama* [2010].

While the above ideas all drew inspiration from numerical simulations and theoretical reasoning, adequate support for these ideas has been lacking. *Romps* [2010] tested some of these ideas in the context of a bulk entraining-detraining plume model and did not find evidence for the $\epsilon \propto 1/z$ relationship or any simple relationship between ϵ and b, or ϵ and db/dz, although it is worth noting that he calculated entrainment and detrainment rates by tracking grid boxes moving in and out of the cloudy updraft category so that his definition of bulk entrainment and detrainment rates differs from the more commonly used effective bulk entrainment and detrainment rates.

One difficulty with diagnosing the relationship between fractional entrainment rate and potential contributing factors, as with all statistical inference, is the effect of confounding: multiple factors that contribute and interfere, making causal inference difficult. To reduce the extent of confounding, we analyze changes in entrainment in response to a small-amplitude temperature perturbation that is horizontally uniform and localized in height. With such a linear response function approach [*Kuang*, 2010], we can identify changes in entrainment characteristics associated with changes in specific environmental conditions while minimizing changes in other environmental conditions as well as changes in cloud characteristics unrelated to the imposed perturbation. This helps to reduce the extent of (but does not eliminate) confounding and allows for more definitive inferences.

The analysis in this paper will be in the framework of an ensemble of entraining plumes of *Arakawa and Schubert* [1974], where plumes are distinguished by their detrainment heights and experience only entrainment (no detrainment) before detrainment. Here the fractional entrainment rates are diagnosed and vary with height instead of being constant in height as assumed in *Arakawa and Schubert* [1974]. We also note that the entraining plume ensembles can be combined to give a bulk entraining-detraining plume [see e.g., *Lawrence and Rasch*, 2005].

Casting the numerically simulated cumulus ensemble in terms of an ensemble of entraining plumes is achieved by tracking Lagrangian particles embedded in large eddy simulations (LES), similar to *Lin and Arakawa* [1997]. The term "entraining plumes" is used here as a way of grouping cloudy updraft parcels in a statistical sense, and they should not be viewed as physical structures such as the similarity plumes in the water tank experiments. Therefore, a "plume" here is a collection of air parcels from different clouds, and parcels from a single cloud contribute to multiple "plumes."

We will focus on nonprecipitating shallow cumuli in this paper. Without the complicating processes associated with precipitation, shallow cumuli are an excellent starting point for studying the cumulus entrainment process. Applications of the present methodology to deep convection will be described in a forthcoming paper.

Section 2 describes the model used and the experimental design. The method of analysis, the results, and their interpretations are presented in section 3, followed by a brief summary in section 4.

2. Models and Experimental Design

The large eddy simulations (LES) were performed with the System for Atmospheric Modeling (SAM) version 6.8.2 [*Khairoutdinov and Randall*, 2001] for the undisturbed phase of the Barbados Oceanographic and Meteorological Experiment (BOMEX) [*Holland and Rasmusson*, 1973]. SAM was run with a doubly periodic domain (6.4 km × 6.4 km) and a horizontal grid spacing of 50 m. There are 128 vertical layers with a 25 m grid spacing. The time step is 1 s. A monotonic advection scheme is used for scalars and the subgrid-scale turbulent fluxes are determined using a 1.5 order closure scheme. The experimental settings of this BOMEX case, such as the initial soundings, the large-scale forcing, and surface fluxes, are the same as those used in *Siebesma et al.* [2003].

We first ran the model for 6 h, with the first 3 h discarded as spin-up. Starting from the end of the third hour, restart files were output every 5 min. A set of 30 min long simulations were initialized from these restart files but with a temperature perturbation added to the initial conditions. The temperature perturbation is horizontally uniform, Gaussian-shaped in height, centered at 975 m with a half width of 75 m and a peak value of +0.25 K (Figure 1). This set of simulations, combined with the initial 6 h long simulation, provides 36 pairs of 30 min long control and perturbed runs in which the perturbed runs start from the same fully developed cumulus fields as the control runs except with the added temperature perturbation. The averaged differences between these pairs of runs are taken as the convective responses to the imposed temperature

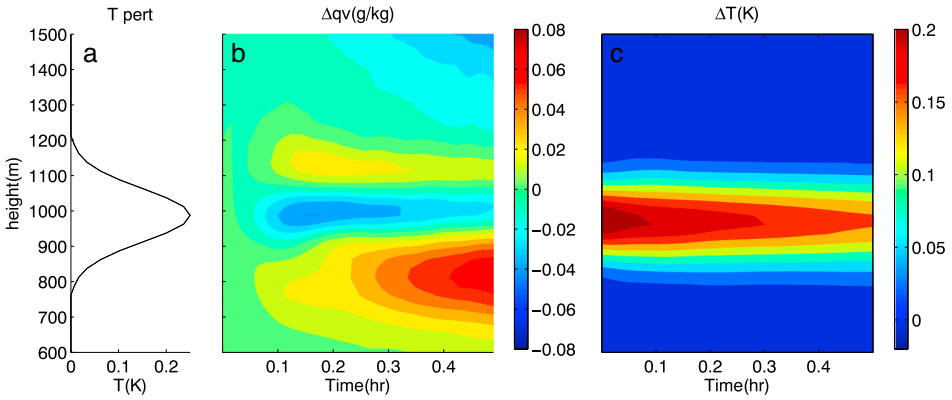

Figure 1. (a) Initial temperature perturbation profile, (b) horizontally averaged moisture anomalies as a function of height and time,(c) same as Figure 1b but for temperature.

perturbation. As convection responds to the temperature anomaly, the amplitude of the initially added temperature anomaly roughly halves over the half hour of simulation, and some moisture anomalies start to develop (Figure 1), similar to *Nie and Kuang* [2012a]. The 30 min simulation length was chosen to allow clouds enough time to respond to the imposed temperature perturbation yet is short enough so that averaged over this time period, the main difference between the horizontally averaged profiles of the control and perturbed experiments remains to be a temperature anomaly localized in height. In future studies, we will impose time-invariant temperature and moisture tendencies to further reduce the evolution of the initially imposed perturbation.

To aid our analysis, we embed a Lagrangian parcel dispersion model (LPDM) into the LES as in *Nie and Kuang* [2012b]. It releases 1600 passive parcels inside each LES vertical column (totaling more than 30 million particles in the LES domain) and advects them based on the LES resolved winds. The release positions of the parcels have a random uniform probability distribution in the horizontal as well as in pressure up to the 2500 m vertical level. Combining the trajectories of the parcels with the snapshots of the LES output provides a full history of parcel properties along their trajectories thus a Lagrangian perspective on cumulus scale dynamics [e.g., *Weil*, 2004; *Heus*, 2008; *Nie and Kuang*, 2012b; *Yeo and Romps*, 2013; *Torri et al.*, 2015]. Some basic validations of the LPDM are included in the supporting information.

3. Analysis and Results

3.1. Response to the Temperature Perturbation

We shall view the simulated cumulus field in the framework of an ensemble of entraining plumes as in, e.g., *Lin and Arakawa* [1997] and *Kuang and Bretherton* [2006]. Grid boxes are considered cloudy updrafts if they have vertical velocities greater than 1 m/s and nonprecipitating liquid water mixing ratios greater than 0.01 g/kg. We then identify grid boxes at 612.5 m, which is just above the cloud base, that are cloudy updrafts and track all parcels within these grid boxes (there are 20 parcels per grid box) until they detrain, where detrainment is defined as parcels exiting cloudy updrafts and not reentering within 1 min [*Nie and Kuang*, 2012b]. We then sort these cloudy updraft parcels that detrain above 762.5 m into 100 groups based on their detrainment heights. For example, among all cloudy updraft parcels that are from 612.5 m and detrain above 762.5 m, the 1% of the parcels that detrain at the highest levels are grouped together as one parcel group (or plume), then the next highest 1% and so on, totaling 100 parcel groups, with larger group numbers indicating higher detrainment heights. The relatively large vertical velocity threshold, compared to, e.g., *Nie and Kuang* [2012a] was chosen to exclude gravity-wave generated vertical fluctuations. Changing the time interval to a longer period (2 min, 3 min, 4 min, or 5 min) does not change the general results. A detrainment height of 762.5 m or higher is imposed to reduce the number of parcels that need to be tracked, as many cloudy updraft parcels from the cloud base detrain at very low altitudes. We will use the terms "parcel group" and "plume" interchangeably as parcel grouping is our way of defining the plumes in the plume ensemble model. Note that the parcel groups defined here were also referred to as subensembles in the literature [e.g., *Lin and Arakawa*, 1997].

With the above definition of parcel groups, we can determine the height range over which the parcels of a particular parcel group detrain (the range can be different between the control and the perturbed experiments). We then identify all cloudy updraft parcels that detrain over this height range (not just those originate from the cloud base). Those parcels that do not originate from the cloud base level are said to have been entrained between the cloud base and their detrainment height. The height of entrainment for a parcel is determined as the height at which the parcel enters a cloudy updraft and does not exit within 1 min. The fractional entrainment rate as a function of height is calculated as the fractional increase in the mass flux carried by all parcels in this parcel group per unit increase in height. Again, the results are not sensitive to the choice of the 1 min time interval.

In addition to properties such as buoyancy, vertical velocity, and total water, we also compute the minimum distance to the cloud edge for each of the grid boxes within the cloudy updraft. The cloud edge is defined to be the horizontal boundary between grid boxes that are cloudy (liquid water greater than 0.01 g/kg) and those that are not. Properties of a parcel are set to be those of the grid box that it resides in (including distance to cloud edge), and properties of a parcel group are given by the averaged properties of all parcels that detrain over the detrainment height range of that parcel group, including parcels originating from cloud base and those entrained later. The choice of a relatively large number (100) of parcel groups is meant to enhance, to some extent, homogeneity within each group while exposing differences among the different groups. Given the chaotic nature of cumulus convection, it is not meaningful to track individual parcels in both control and perturbed runs and analyze changes in their behaviors due to the perturbation. Using our method of parcel grouping, parcels belonging to the same parcel group in the control and perturbed runs may be viewed as the same parcels in a statistical sense.

Figure 2 shows parcel group properties in the control runs (Figures 2a–2e) and their changes in the perturbed runs relative to the control (Figures 2f–2j) as functions of parcel group number (x axis) and height (y axis). Figures 2a and 2c show that buoyancy and total water content at the cloud base are uniform across the different parcel groups, while Figures 2b and 2d show that a parcel that detrains higher tends to start at the cloud base slightly further away from the cloud edge and with slightly higher vertical velocity, indicating some roles of initial conditions in determining the fate of cloudy updrafts. Figure 2e shows that parcel groups that reach higher tend to have smaller fractional entrainment rate. These parcels become increasingly more positively buoyant with higher vertical velocity during their ascent relative to those parcels that detrain at lower heights (smaller group numbers), which possess smaller positive buoyancy up to their detrainment levels. The vertical velocity of the highest reaching parcel groups can reach up to 4 m/s as they enter the base of the trade inversion (around 1500 m). After that point, the buoyancy acceleration begins to decrease. Total water content decreases monotonically with height for all parcel groups but more slowly for the higher-reaching ones. These results are consistent with those of *Romps and Kuang* [2010], who showed that in-cloud heterogeneity is mostly caused by the stochastic nature of the entrainment process, not the initial conditions at the cloud base. As such, their conclusion was that initial conditions at the cloud base have no *dominant control* on the fate of cloudy updrafts but did not exclude the possibility that initial conditions at the cloud base can have some influence on the fate of cloudy updrafts. As discussed later in the next section, differences in entrainment rates among the different parcel groups near the cloud base likely come from the stochastic nature of the entrainment process, which implies that the different parcel groups are mostly a measure of how "lucky" the parcels are in avoiding dilution from entrainment.

We now focus on those parcel groups that are most affected by the added perturbation (parcel group 75 and higher) and examine their responses to the perturbation; the other parcel groups detrain at lower altitudes and do not experience the full effect of the added perturbation. The imposed warm anomaly forms a buoyancy barrier, shown as a belt of negative buoyancy anomalies in the perturbed layer (Figure 2f). The change in vertical velocity (Figure 2g) is consistent with that of buoyancy acceleration: updraft vertical velocity decreases inside and above the perturbed region with less reduction for the highest reaching parcels, which experience smaller buoyancy reduction because they traverse the barrier more quickly. In this nonprecipitating shallow cumulus case, total water is a conserved quantity. The slight increase of total water content in the perturbed region and its decrease above is the result of changes in the entrainment. Overall, the results here are consistent with those in *Nie and Kuang* [2012a]. A full discussion of the underlying mechanisms of these responses from a Lagrangian perspective will be presented in a separate paper. Below we shall focus on the entrainment process.

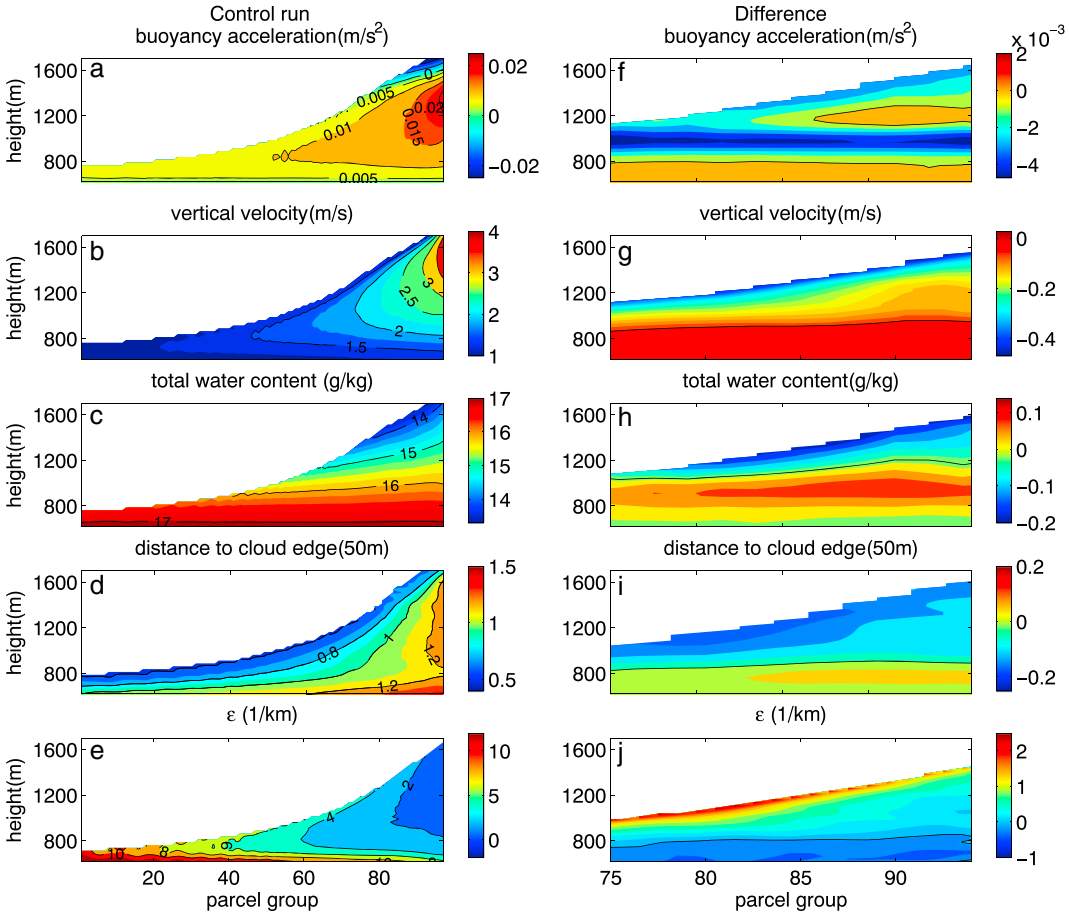

Figure 2. Control run cloudy updraft (a) buoyancy acceleration, (b) vertical velocity, (c) total water content, (d) distance to the cloud edge (with the unit of grid spacing), (e) fractional entrainment rate ϵ per kilometer, as functions of parcel group and height (see text for details on how the parcel groups are defined); (f–j) The same as Figures 2a–2e but for the differences between the ensemble perturbed and control runs. Solid black curve delineates the zero contour line.

3.2. Dependence of Entrainment on Vertical Velocity and Distance to Cloud Edge

Cloudy updrafts in the control and the perturbed cases have similar characteristics at the cloud base, as evidenced by the small differences at the cloud base seen in Figures 2f–2j. Above the cloud base, the cloudy updrafts entrain slightly less (per unit height) in the lower portion of the added temperature perturbation (one half width below the peak of the perturbation, or below ~900 m) and entrain more at higher altitudes in the perturbed runs (Figure 2j). There are a number of ways that the warm anomaly may change the entrainment process. The warm anomaly increases the stratification below the peak of the perturbation and decreases it above, thus modifying the vertical gradient of cloud buoyancy which has been argued to be a control on entrainment [*Emanuel and Zivkovic-Rothman*, 1999]. The added warm anomaly also reduces cloud buoyancy (Figure 2f) and environmental relative humidity, which were suggested by *Lin* [1999] and *Bechtold et al.* [2008], respectively, to enhance entrainment. Other factors that may contribute to the strong entrainment above the perturbation layer are slower cloudy updrafts and smaller distance to the cloud edge. It takes the slower cloudy updrafts (Figure 2g) more time to traverse a given distance compared to the faster ones, which give them more time to entrain environmental air, resulting in more entrainment per unit height, an argument made previously by *Neggers et al.* [2002]. Furthermore, as less buoyant cloudy parcels get stripped away (detrained) from the outer rim of the clouds by the imposed buoyancy barrier, clouds become smaller (Figure 2i). This exposes the cloud cores to greater amounts of entrainment.

As a representative example, Figure 3 shows the percentage changes in updraft vertical velocity, distance to cloud edge, and stratification for parcel group 80. Changes in w are monotonic in height, whereas changes in stratification (and the vertical gradient in cloud buoyancy) are antisymmetric about the peak of the

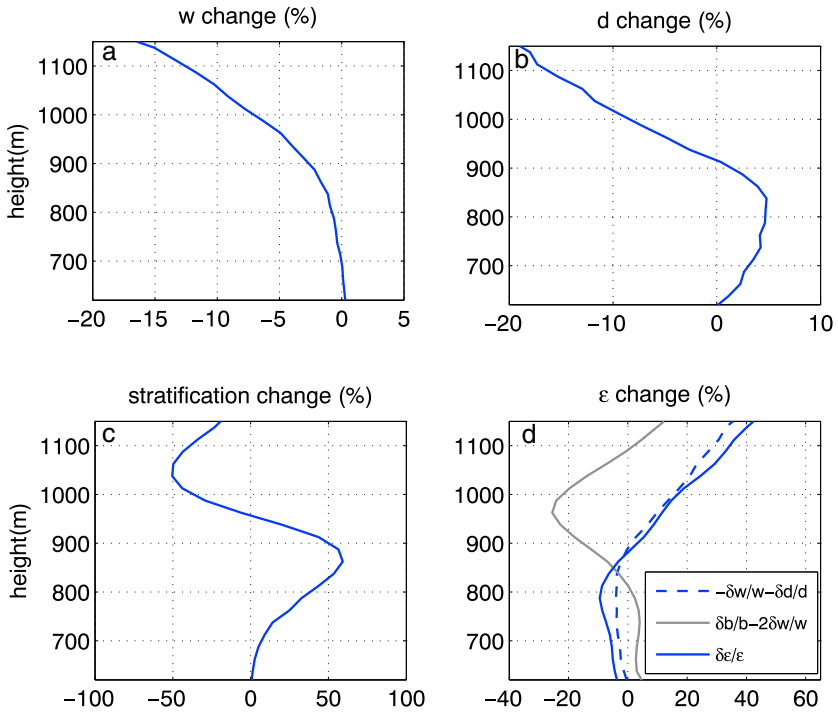

Figure 3. Percentage change in (a) vertical velocity (w), (b) distance to the cloud edge (d), (c) stratification, and (d) fractional entrainment rate (ϵ) for parcel group 80. The sum of the percentage changes in vertical velocity and distance to cloud edge with the sign reversed is also plotted in Figure 3d; the gray line denotes the sum of the percentage changes in buoyancy and vertical velocity, which corresponds to the empirical relation proposed by *Gregory* [2001]. Stratification is calculated as $d\theta_\rho/dz$, θ_ρ is the density potential temperature which takes into account water loading in calculating parcel densities. Distance to the cloud edge is calculated as the minimum distance to the cloud edge.

temperature perturbation. Changes in cloud buoyancy and environmental relative humidity take a form similar to the added temperature anomaly (but opposite in sign) and are also not consistent with changes in ϵ. These comparisons indicate that for the present case, changes in cloud buoyancy, vertical gradient of cloud buoyancy, and environmental relative humidity, are not of the first-order importance to changes in the entrainment rates (defined in the framework of an ensemble of entraining plumes). Figure 3d shows that relative changes in the fractional entrainment rate of a parcel group can be reproduced to a good extent by adding the relative changes in w and d with reversed signs. In other words, our result implies the following local relationship:

$$\epsilon_i = \frac{\alpha_i}{w_i d_i} \tag{1}$$

where the subscript i is used to highlight the fact that this relationship applies to individual parcel groups.

The velocity scale α_i can potentially vary among the parcel groups and heights but remains the same with or without the temperature perturbation. Distance to the cloud edge d_i increases below the perturbation layer and decreases above it. The decrease in d_i above the perturbation layer, as argued earlier, can be expected since the less buoyant cloudy parcels are detrained from the outer rim of the clouds because of the buoyancy barrier. The reason for the increase in d_i below the perturbation is less clear. It is possible that the stronger stratification there causes the clouds to spread more horizontally, giving stratification an indirect role in entrainment. But it is also possible that the increase in d_i is caused by changes in the convective fields below the perturbation layer during the 30 min period after the imposition of the temperature anomaly. Further studies to resolve this are warranted. Figure 3d also shows that $\delta b_i/b_i - 2\delta w_i/w_i$ does not reproduce $\delta\epsilon_i/\epsilon_i$. Therefore, the formula $\epsilon_i \propto \frac{b}{w_i^2}$ proposed by *Gregory* [2001] in the context of a bulk entraining-detraining plume model and used in an entraining plume ensemble model by *Chikira and Sugiyama* [2010] is not supported by the present results.

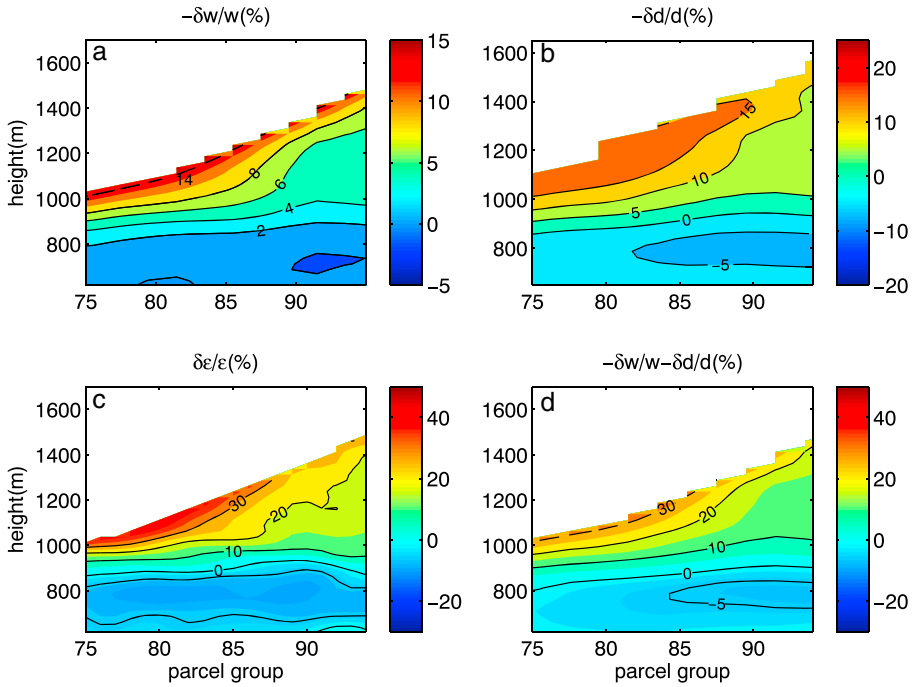

Figure 4. Percentage change in (a) vertical velocity, (b) distance to cloud edge, and (c) fractional entrainment rate ϵ diagnosed from the model. (d) The sum of the percentage changes in vertical velocity and in distance to cloud edge with the sign reversed.

The same analyses for all higher-reaching parcel groups are shown in Figure 4. Comparing the diagnosed ϵ_i changes from model output and calculated changes using equation (1), we see that this relationship can capture the main features of ϵ_i changes quite well.

Based on the above suggested relationship, we calculated α_i for both cases (Figure 5). α_i has some variations and in particular is higher close to the cloud base and for parcel groups that detrain at low altitudes. This implies that close to the cloud base, variations in ϵ_i across the different parcel groups are not explained by equation (1). On the other hand, within the bulk of the cloud layer that we examined (between 900 m and 1400 m), α_i does not vary much with height or with parcel group and takes the value of ~0.23 m/s. The values of α_i also do not change much between the perturbed and control cases, consistent with the inference from Figures 3 and 4. Setting α_i in equation (1) to 0.23 m/s reproduces model diagnosed ϵ_i over this height range quite well (results not shown here). The velocity scale α_i is determined entirely empirically here but may scale with the square root of the turbulent kinetic energy, as greater turbulent kinetic energy is expected to produce stronger mixing and entrainment. Such a possibility will be investigated in future studies.

The inverse relationship between ϵ_i and w_i was suggested previously by *Neggers et al.* [2002] and was argued to lead to a positive feedback that amplifies the cloud-base differences and produces the in-cloud heterogeneity seen in the Paluch diagram [*Paluch*, 1979]. The current results support the inverse relationship suggested by *Neggers et al.* [2002] but not its dominant role in explaining the in-cloud heterogeneity, which, as shown in *Krueger et al.* [1997], is a consequence discrete entrainment events and finite-rate turbulent mixing. The inverse relationship between ϵ_i and w_i implies that the entrainment inflow velocity (or fractional entrainment rate per unit time) is constant instead of being proportional to the updraft velocity, the latter being the case in the similarity plumes of, for example, *Morton et al.* [1956]. We offer the following speculations for the possible cause of this difference. In similarity plumes, turbulent mixing, vertical velocity, and buoyancy of the whole plume are tied together through the similarity relationship. In contrast, based on numerical simulations of cumulus clouds, *Grabowski and Clark* [1991, 1993], for example, have suggested that evaporative cooling can create a strong density gradient across the cloud-environment interface, and the interaction between the strong density gradient and the shear zone across this interface is important for eddy growth, turbulent mixing, and entrainment into the clouds. Therefore, entrainment inflow velocity (or fractional entrainment

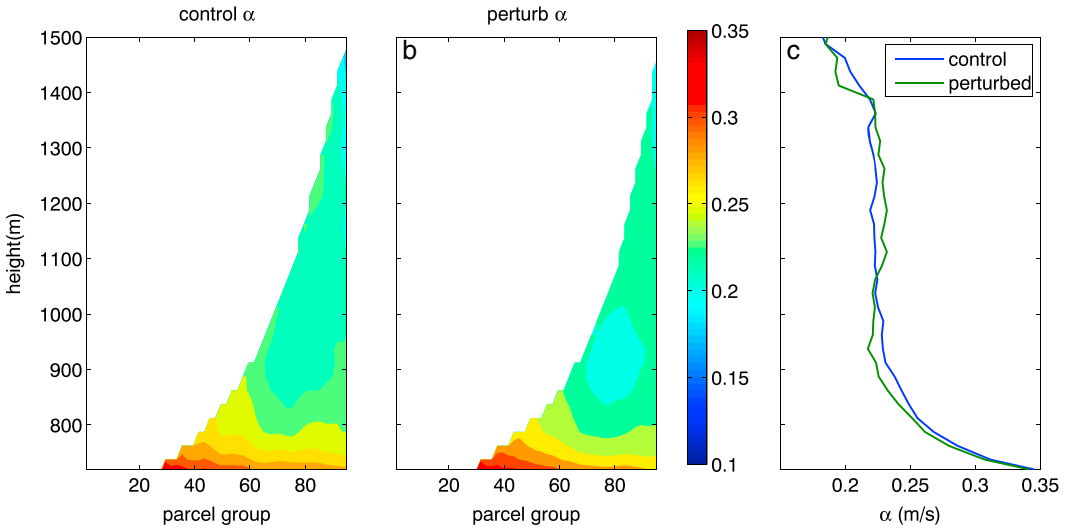

Figure 5. (a) Coefficients α determined from equation (1) using ϵ, w, and distance to the cloud edge diagnosed from the control runs, (b) Same as Figure 5a but for the perturbed runs, (c) α values averaged across all parcel groups as a function of height.

rate per unit time) in cumulus clouds may be strongly controlled by the evaporative cooling and density-shear interaction across the cloud-environment boundary instead of being directly tied to the updraft velocity.

4. Summary and Discussions

We have investigated how entrainment rates of shallow cumuli depend on environmental conditions and cloud characteristics by examining their responses to a small-amplitude temperature perturbation that is horizontally uniform and localized in height. This allowed us to identify changes in entrainment rates associated with specific environmental conditions while minimizing changes in other environmental conditions as well as cloud characteristics unrelated to the imposed perturbation. We analyzed the simulated cumulus ensemble in terms of an ensemble of entraining plumes by tracking a large number of Lagrangian parcels embedded in the LES. Partitioning cloudy updraft parcels into different groups based on their eventual detrainment heights provided that plume ensemble view. We found that in response to the imposed warm anomaly, cloudy updraft parcels entrain slightly less in the lower portion of the perturbed layer and entrain considerably more above the peak perturbation level. Changes in the fractional entrainment rate of the ith parcel group ϵ_i are quite well described by a simple inverse relationship between ϵ_i and the vertical velocity w_i and the distance to the cloud edge of that parcel group (equation (1)). The proportionality factor α_i, tentatively interpreted as a turbulent velocity scale, is nearly constant ($\sim$ 0.23 m/s) over the bulk of the cloud layer (900–1400 m). In addition, α_i does not differ much between the control and perturbed cases and setting it to 0.23 m/s seems to reproduce entrainment rates quite well over the bulk of the cloud layer in this shallow convection case (BOMEX). While our analyses and results are for an ensemble of entraining plumes, the entraining plume ensembles can be combined to give a bulk entraining-detraining plume [see, e.g., *Lawrence and Rasch*, 2005].

A major emphasis of this paper is to describe our Lagrangian tracking-based analysis of linear response functions of convection and to illustrate its value in gaining insight into the underlying dynamics. To that end, we have focused on the effects of an imposed temperature perturbation, which emphasizes certain aspects of convection because of its effect as a buoyancy barrier. Imposing other types of perturbations may allow tests that are better tailored to other aspects of the convection. For example, a small-amplitude moisture perturbation that is horizontally uniform and localized in height may allow a closer analysis of the effect of environmental relative humidity with less influence from the buoyancy barrier effect. Such additional experiments could be valuable, although we do note that responses to such a moisture anomaly have been found to be weak in the BOMEX case [*Nie and Kuang*, 2012a]. Since analyses and results in the present paper are based on the specific case of BOMEX, studies of additional cases are clearly warranted to generalize the results.

Some aspects of the present simulations shall be improved in future studies. As the typical effective radius of the simulated clouds is 150 to 200 m (see supporting information), the numerical resolution used in this

study (dx=dy = 50 m, dz = 25 m), while finer than that adopted in the BOMEX LES intercomparison study of *Siebesma et al.* [2003] (dx = dy = 100 m and z = 40 m), does not resolve most of the entraining eddies across the cloud-environment interface. Entrainment in the simulations therefore depends on the SGS closure and does not account for SGS heterogeneity in mixing , leaving open the possibility of too rapid SGS mixing and evaporation. *Nie and Kuang* [2012a, 2012b], using the SAM model, found that the linear response functions and the mixing characteristics of the BOMEX case were robust when resolutions were varied from dx = dy = dz = 25 m to dx = dy = 100 m, dz = 50 m. While that lends some confidence to our results, it is desirable to repeat our simulations and analyses using higher resolutions in future studies so that the entraining eddies can be better resolved. In addition to numerical resolution, *Jarecka et al.* [2009, 2013] also explored more sophisticated SGS closures to account for the heterogeneity of SGS mixing and found that with resolution similar to that used in the present study, the effect of the more sophisticated SGS closures is somewhat limited, and the effect of heterogeneity in SGS mixing is small. *Jarecka et al.* [2013] argued that the latter is because the environmental air entrained into trade cumuli is already close to saturation (in contrast to the case of stratocumulus). However, it is not yet clear whether their SGS closures are adequate, and combining an approach such as the linear eddy model [*Krueger et al.*, 1997] and the LES may be necessary to more fully address the issue of SGS mixing and evaporation. As noted in sections 2 and 3, there is also some drift in the horizontally averaged sounding over the 30 min period that we analyze (Figure 1), complicating the interpretation. Future studies will employ time-invariant forcings to minimize such drifts. Lastly, we note that the same methodology can be applied to deep convection, and the results will be reported in a forthcoming publication.

Acknowledgments
This research was partially supported by the Office of Biological and Environmental Research of the U.S. DOE under grant DE-SC0008679 as part of the ASR Program, NOAA grant NA13OAR4310154, and NSF grant AGS-1260380. The authors thank Marat Khairoutdinov for making the SAM model available, Martin Singh, Giuseppe Torri, Pedram Hassanzadeh for valuable comments, and Steve Krueger, Roel Neggers for very helpful reviews. The Harvard Odyssey cluster provided much of the computing resources for this study.

References

Arakawa, A., and W. H. Schubert (1974), Interaction of a cumulus cloud ensemble with the large-scale environment. Part I, *J. Atmos. Sci.*, *31*, 674–701.

Bechtold, P., M. Kohler, T. Jung, F. Doblas-Reyes, M. Leutbecher, M. J. Rodwell, F. Vitart, and G. Balsamo (2008), Advances in simulating atmospheric variability with the ECMWF model: From synoptic to decadal time-scales, *Q. J. R. Meteorol. Soc.*, *34*, 1337–1351.

Bretherton, C. S., and P. K. Smolarkiewicz (1989), Gravity Waves, compensating subsidence, and detrainment around cumulus clouds, *J. Atmos. Sci.*, *46*, 740–759.

Bretherton, C. S., J. R. McCAA, and H. Grenier (2004), A new parameterization for shallow cumulus convection and its application to marine subtropical cloud-topped boundary layers. Part I: Description and 1D results, *Mon. Weather Rev.*, *132*, 864–882.

Chikira, M., and M. Sugiyama (2010), A cumulus parameterization with state-dependent entrainment rate. Part I: Description and sensitivity to temperature and humidity profiles, *J. Atmos. Sci.*, *67*, 2171–2193.

Dawe, J. T., and P. H. Austin (2013), Direct entrainment and detrainment rate distributions of individual shallow cumulus clouds in an LES, *Atmos. Chem. Phys.*, *13*, 7795–7811.

Emanuel, K. A., and M. Zivkovic-Rothman (1999), Development and evaluation of a convection scheme for use in climate models, *J. Atmos. Sci.*, *56*, 1766–1782.

Grabowski, W. W., and T. L. Clark (1991), Cloud-environment interface instability: Rising thermal calculations in two spatial dimensions, *J. Atmos. Sci.*, *48*, 527–546.

Grabowski, W. W., and T. L. Clark (1993), Cloud-environment interface instability: Part II: Extension to three spatial dimensions, *J. Atmos. Sci.*, *50*, 555–573.

Grant, A. L. M., and A. R. Brown (1999), A similarity hypothesis for shallow-cumulus transports, *Q. J. R. Meteorol. Soc.*, *125*, 1913–1936.

Gregory, D. (2001), Estimation of entrainment rate in simple models of convective clouds, *Q. J. R. Meteorol. Soc.*, *127*, 53–72.

Hohenegger, C., and C. S. Bretherton (2011), Simulating deep convection with a shallow convection scheme, *Atmos. Chem. Phys.*, *11*, 10,389–10,406.

Heus, T. (2008), Mixing in shallow cumulus clouds studied by Lagrangian particle tracking, *J. Atmos. Sci.*, *65*, 2581–2597.

Holland, J. Z., and E. M. Rasmusson (1973), Measurement of atmospheric mass, energy, and momentum budgets over a 500-kilometer square of tropical ocean, *Mon. Weather Rev.*, *101*, 44–55.

Jarecka, D., W. W. Grabowski, and H. Pawlowska (2009), Modeling of subgrid-scale mixing in large-eddy simulation of shallow convection, *J. Atmos. Sci.*, *66*, 2125–2133.

Jarecka, D., W. W. Grabowski, and H. Pawlowska (2013), Homogeneity of the subgrid-scale turbulent mixing in large-eddy simulation of shallow convection, *J. Atmos. Sci.*, *70*, 2751–2767.

Krueger, S. K., C.-W. Su, and P. A. McMurtry (1997), Modeling entrainment and fine-scale mixing in cumulus clouds, *J. Atmos. Sci.*, *54*, 2697–2712.

Kuang, Z. (2010), Linear response functions of a cumulus ensemble to temperature and moisture perturbations and implication to the dynamics of convectively coupled waves, *J. Atmos. Sci.*, *67*, 941–962.

Kuang, Z. (2012), Weakly forced mock walker cells, *J. Atmos. Sci.*, *69*, 2759–2786.

Kuang, Z., and S. C. Bretherton (2006), A mass-flux scheme view of a high-resolution simulation of a transition from shallow to deep cumulus convection, *J. Atmos. Sci.*, *63*, 1895–1909.

Khairoutdinov, M. F., and D. A. Randall (2001), A cloud-resolving model as a cloud parameterization in the NCAR community climate system model: Preliminary results, *Geophys. Res. Lett.*, *28*, 3617–3620.

Lawrence, M. G., and P. J. Rasch (2005), Tracer transport in deep convective updrafts: Plume ensemble versus bulk formulations, *J. Atmos. Sci.*, *62*, 2880–2894.

Lin, C. (1999), Some bulk properties of cumulus ensembles simulated by a cloud-resolving model. Part II: Entrainment profiles, *J. Atmos. Sci.*, *56*, 3736–3748.

Lin, C., and A. Arakawa (1997), The macroscopic entrainment processes of simulated cumulus ensemble. Part II: Testing the entraining-plume model, *J. Atmos. Sci.*, *54*, 1044–1053.

Mapes, B., and R. Neale (2011), Parameterizing convective organization to escape the entrainment dilemma, *J. Adv. Model. Earth Syst.*, *3*, M06004, doi:10.1029/2011MS000042.
Morton, B., G. Taylor, and J. Turner (1956), Turbulent gravitational convection from maintained and instantaneous sources, *Proc. R. Soc. A*, *234*, 1–23.
Neggers, R. A. J., A. P. Siebesma, and H. J. J. Jonker (2002), A multipacel model for shallow cumulus convection, *J. Atmos. Sci.*, *59*, 1655–1668.
Nie, J., and Z. Kuang (2012a), Responses of shallow cumulus convection to large-scale temperature and moisture perturbations: A comparison of large-eddy simulations and a convective parameterization based on stochastically entraining parcels, *J. Atmos. Sci.*, *69*, 1936–1956.
Nie, J., and Z. Kuang (2012b), Beyond bulk entrainment and detrainment rates: A new frame-work for diagnosing mixing in cumulus convection, *Geophys. Res. Lett.*, *39*, L21803, doi:10.1029/2012GL053992.
Paluch, I. R. (1979), The entrainment mechanism in Colorado cumuli, *J. Atmos. Sci.*, *36*, 2467–2478.
Raymond, D. J., and A. M. Blyth (1986), A stochastic mixing model for nonprecipitating cumulus clouds, *J. Atmos. Sci.*, *43*, 2708–2718.
Romps, D. M. (2010), A direct measure of entrainment, *J. Atmos. Sci.*, *67*, 1908–1927.
Romps, D. M., and Z. Kuang (2010), Do undiluted convective plumes exist in the upper tropical troposphere?, *J. Atmos. Sci.*, *67*, 468–484.
Siebesma, A. P. (1998), Shallow cumulus convection, in *Buoyant Convection in Geophysical Flows*, edited by E. J. Plate et al., pp. 441–486, Kluwer Acad., Dordrecht, Netherlands.
Siebesma, A. P., et al. (2003), A large eddy simulation inter comparison study of shallow cumulus convection, *J. Atmos. Sci.*, *60*, 1201–1219.
Simpson, J., and V. Wiggert (1969), Models of precipitating cumulus towers, *Mon. Weather Rev.*, *97*, 471–489.
Tiedtke, M. (1989), A comprehensive mass flux scheme for cumulus parameterization in large-scale models, *Mon. Weather Rev.*, *117*, 1779–1800.
Torri, G., Z. Kuang, and Y. Tian (2015), Mechanisms for convection triggering by cold pools, *Geophys. Res. Lett.*, *42*, 1943–1950.
Weil, J. C. (2004), The use of large-eddy simulation in Lagrangian particle dispersion models, *J. Atmos. Sci.*, *61*, 2877–2887.
Yeo, K., and D. Romps (2013), Measurement of convective entrainment using Lagrangian particles, *J. Atmos. Sci.*, *70*, 266–277.